

# Space as a low-temperature regime of graphs

Florian Conrady\*

*Perimeter Institute for Theoretical Physics, Waterloo, Ontario, Canada*

I define a statistical model of graphs in which 2-dimensional spaces arise at low temperature. The configurations are given by graphs with a fixed number of edges and the Hamiltonian is a simple, local function of the graphs. Simulations show that there is a transition between a low-temperature regime in which the graphs form triangulations of 2-dimensional surfaces and a high-temperature regime, where the surfaces disappear. I use data for the specific heat and other observables to discuss whether this is a phase transition. The surface states are analyzed with regard to topology and defects.

## I. INTRODUCTION

Spacetime represents one of the remaining frontiers in theoretical physics. We have successful theories of fields *in* spacetime and of the geometry *of* spacetime. But there is no established theory of spacetime itself, a theory that would explain why we live in a spacetime and not in something completely different.

There are approaches that go in this direction, notably string theory, matrix models [1]–[4], twistor theory [5, 6], causal dynamical triangulations [7, 8], Regge calculus [9], loop quantum gravity [10–12] and quantum graphity [13]–[18]. Some of these start from objects that are radically different from spacetime and one hopes that spacetime arises from the dynamics of these objects. In others, spacetime is assumed from the beginning and only the topology and geometry is dynamical.

In this article, I am concerned with the former type of approach, i.e. the attempt to obtain space from a theory, where there is no space to start with. I define a simple statistical model of graphs that is designed to have 2-dimensional triangulations as ground states. The setup is close in spirit to earlier models of quantum graphity explored by Konopka, Markopoulou, Smolin and others [13]–[18]. I present data from Monte Carlo simulations<sup>1</sup> of graphs with 45, 90 and 180 edges. The results show that the system settles into 2d triangulations at low temperatures. Above a transition temperature the surface states disappear and more general graphs dominate. As far as I know, this is the first time that a model of graphs succeeds in reaching manifold-like states without help from additional ad hoc constraints. The temperature dependence of specific heat and other observables exhibits similar features as in phase transitions of more conventional systems. The transition temperature, however, drifts as the size of the system is changed, leaving both a finite- and zero-temperature phase transition as a possible scenario for the infinite-size limit.

In a second set of simulations, I investigated the surface properties in more detail with regard to topology, defects and curvature. At very low temperature the surfaces are typically

---

\*Electronic address: fconrady@perimeterinstitute.ca

<sup>1</sup> For an introduction to Monte Carlo methods, see e.g. [19].

connected and non-orientable, and carry a number of conical singularities.

In the space of graphs the surface states form a very complex subset. Like in other systems with a complex energy landscape (see e.g. [20–22]), this makes it difficult to ensure equilibrium at low temperature. The simulation may get trapped in energy valleys and sample no longer according to the Boltzmann distribution. To check whether the simulation is equilibrated, I compare the original simulation with an alternate simulation schedule that involves frequent restarts and annealing.

Although triangulations play a role in this model, the setup is quite different from causal dynamical triangulations and Regge calculus. In these theories, each individual configuration is a space in the form of a triangulation, and one finds different regimes, where the effective geometry is smooth, crumbled or polymer-like, for example. In our case, the configurations are graphs and the regimes are distinguished by the existence or absence of a space.

For testing and inspecting the simulation I used the Ubigraph software for visualizing dynamic graphs [23]. Videos of the simulation can be viewed at this link [24].

The paper is organized as follows. In section II I define the model and discuss the expected ground states and its defects. I also define an observable used to measure the “superficiality” of graphs. Section III describes the details of the algorithm—the Monte Carlo moves and the trial probabilities needed for detailed balance. This is followed by sec. IV, where I report the results of the simulation. I discuss evidence for and against a phase transition and the graphs’ properties at low temperature. The question of low temperature equilibration is scrutinized in sec. V. In the final section, I give a summary and discuss some of the conceptual aspects of the model.

## II. THE MODEL

### A. Definition

The model is a statistical model of graphs. Configurations are given by undirected, labelled graphs  $\Gamma$  with a fixed number  $N_e$  of edges. The edges of the graphs are labelled by numbers  $1, 2, \dots, N_e$ . Automorphic graphs are distinguished if they differ in their labelling of edges. Vertices have to be contained in at least one edge. There can be at most one edge between two vertices, i.e. double, triple etc. edges are not allowed. Moreover, edges from a vertex to itself are prohibited.

Vertices and edges of graphs are denoted by  $v$  and  $e$  respectively. When  $n + 1$  vertices form a complete subgraph (i.e. when every vertex of the subgraph is connected with each of its other vertices), I call this subgraph an  $n$ -simplex. Thus, vertices and edges define 0- and 1-simplices. 2- and 3-simplices will be referred to as triangles  $t$  and tetrahedra  $\tau$  respectively. For the definition of the Hamiltonian the notion of *valence* is important. An  $n$ -simplex  $\Delta$  is said to have valence  $V_\Delta$ , if it is contained in  $V_\Delta$   $(n + 1)$ -simplices.

The Hamiltonian is specified in such a way that it favors graphs corresponding to a 2-dimensional triangulation. That is, graphs are energetically preferred when its subgraphs form simplices of a 2-dimensional simplicial complex. The Hamiltonian depends on the graph  $\Gamma$  and is a sum of four types of terms that are associated to vertices, edges, triangles and tetrahedra:

$$H_\Gamma = \sum_v H_v + \sum_e H_e + \sum_t H_t + \sum_\tau H_\tau \quad (1)$$

The sums extend over all vertices  $v$ , edges  $e$ , triangles  $t$  and tetrahedra  $\tau$  contained in  $\Gamma$ . The individual terms are defined as follows:

$$H_v = c_v |V_v - 6|, \quad H_e = \begin{cases} 0, & V_e \leq 2, \\ c_e V_e^2, & V_e > 2, \end{cases}, \quad H_t = -c_t, \quad H_\tau = c_\tau. \quad (2)$$

The coefficients  $c_v$ ,  $c_e$ ,  $c_t$  and  $c_\tau$  are positive constants and their specific values are taken to be

$$c_v = 1, \quad c_e = 10, \quad c_t = 7, \quad c_\tau = 500. \quad (3)$$

The most important terms are  $H_e$  and  $H_t$ . The triangle term  $H_t$  favors the creation of triangles, since every triangle lowers the energy by  $c_t$ . The edge term  $H_e$  penalizes edges with a valence  $V_e$  greater than 2. It thus suppresses the branching of triangles, which would be incompatible with a 2d triangulation. The tetrahedral term  $H_\tau$  suppresses the formation of tetrahedra and allows us to exclude surfaces that consist merely of disconnected tetrahedra. The vertex term  $H_v$  was introduced in order to favor smooth, low-curvature triangulations over rough, and crumbled ones<sup>2</sup>. The curvature at a vertex  $v$  is determined by its valence  $V_v$ , and in 2 dimensions a valence of 6 corresponds to flatness.

The partition function is defined by

$$Z = \sum_{\Gamma} e^{-\beta H_{\Gamma}}, \quad (4)$$

where  $\beta$  is the inverse of the temperature  $T$ . The sum includes all graphs with  $N_e$  edges that are admissible according to the rules stated previously. The average of an observable  $O_{\Gamma}$  is given by

$$\langle O \rangle = \frac{1}{Z} \sum_{\Gamma} O_{\Gamma} e^{-\beta H_{\Gamma}}. \quad (5)$$

## B. Surfaces, defects and their observables

The above choice of the Hamiltonian makes it likely that triangulations of surfaces are among the ground states of the system. Surfaces, in the strict sense, need not be the only minima of energy, however, since there can occur defects to which the Hamiltonian is not sensitive.

Through the identification of complete subgraphs with simplices, each admissible graph  $\Gamma$  defines a simplicial complex. A simplicial complex is a triangulation of a surface (with boundary) if and only if<sup>3</sup>

- (a) all edges have valence  $V_e = 1$  or  $V_e = 2$ , and
- (b) at every vertex edges and triangles form a sequence  $e_1 t_1 e_2 t_2 e_3 \dots e_n t_n e_{n+1}$ , where  $e_i, e_{i+1} \subset t_i$  (and  $e_1 = e_{n+1}$  or  $e_1 \neq e_{n+1}$ ).

<sup>2</sup> As such a triangulation defines only a topological manifold, but if we think of each edge as having the length 1, it becomes a manifold with a metric, i.e. a manifold with a notion of distance and curvature.

<sup>3</sup> see e.g. [25], sec. I.4.22

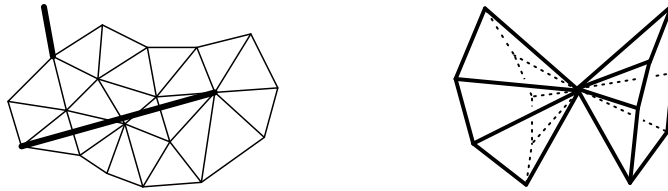


Figure 1: Defects: edges with valence  $V_e = 0$  and conical singularities.

The term  $H_e$  in the Hamiltonian (1) does not distinguish between valence  $V_e = 1, 2$  and  $V_e = 0$ , so there could be minima that consist of surfaces dressed with additional edges outside of any triangle (see Fig. 1). The term  $H_t$  tends to eliminate these edges in order to maximize the number of triangles for a given total edge number  $N_e$ . Nevertheless there could remain edges as “odd men out”, since their inclusion would require a restructuring of the triangulation. The analysis is further complicated by the term  $H_v$ , which is sensitive to the valence of vertices. Finally, even when condition (a) is fulfilled, the simplicial complex may not be a surface, because condition (b) is violated at one or several vertices. Such vertices correspond to so-called conical singularities, where two surfaces are joined in a single point (see Fig. 1).

For these reasons, it is difficult to state precisely which graphs are the minima of energy. The previous arguments suggest that the ground state is given by surfaces with defects in the form of conical singularities and edges with valence  $V_e = 0$ .

The purpose of the present work is to determine by simulation whether this intuitive picture is correct and if the system does indeed settle into surface-like states at low temperatures. Moreover, this should allow one to see how the system departs from these states as the temperature is increased. To quantify the presence (or absence) of a surface, I use an observable  $M$  that measures how close the graph is to being a triangulation of a 2d manifold:

$$M \equiv \sum_e m_e, \quad m_e \equiv \begin{cases} 0, & V_e = 0, \\ 1/2, & V_e = 1, \\ 1, & V_e = 2, \\ 0, & V_e > 2. \end{cases} \quad (6)$$

Edges with valence  $V_e = 2$  contribute with 1 to  $M$ , boundary edges add 1/2 and any other edge counts as zero. When comparing systems of different size  $N_e$ , it is convenient to use the “intensive” quantity

$$m \equiv \frac{1}{N_e} M. \quad (7)$$

A graph with  $m = 1$  is, up to conical singularities, a perfect surface without boundary. As  $m$  is not sensitive to conical singularities, the number  $N_{\text{con}}$  of such singularities is another observable that will be measured in the simulation. By analogy to the susceptibility of a magnet, I will also define and measure a “susceptibility” related to  $M$ :

$$\chi \equiv \frac{\beta}{N_e} (\langle M^2 \rangle - \langle M \rangle^2) = \beta N_e (\langle m^2 \rangle - \langle m \rangle^2) \quad (8)$$

### III. MONTE CARLO SIMULATION

I simulated the model by the Monte Carlo method using a Metropolis algorithm. In setting up this simulation the main challenge was to find suitable moves that allow one to explore the states of the system efficiently at low temperatures. One can adopt a very simple set of moves that displace edges randomly from one location to another, and such moves would be clearly ergodic. It is far from clear, however, that these moves are also powerful enough to sample all the relevant configurations within a limited simulation time. The surface configurations deemed to be important at low temperature constitute only a tiny fraction of the full space of graphs. It is doubtful that a mere hit and miss method can reach these very special graphs. Initial simulations showed, in fact, that such minimal moves are not sufficient for finding these configurations.

To resolve this problem I extended this set of moves by more elaborate moves that assist the system in building low-energy configurations. The resulting algorithm succeeds in sampling the surface graphs<sup>4</sup>.

In the next two subsections, I describe the moves of this algorithm and also the trial probabilities that are needed to achieve detailed balance.

#### A. Moves

Since the number  $N_e$  of edges is conserved, each Monte Carlo move consists of a succession of two more basic moves. The first move removes  $m$  edges from the graph and the second one adds again  $m$  edges.

I found it convenient to categorize these moves into 6 types, labelled by a pair of numbers  $n_m$ . The number  $m$  denotes the change in the number of edges, while  $n$  labels the specific way in which the addition (or removal) of edges happens (see Fig. 2).

Roughly speaking,  $n_m$ ,  $m > 0$ , stands for a move that creates a new simplex by adding  $m$  edges. If  $n = 1$ , this is done by adding a new simplex that is disconnected from the rest of the graph. If  $n = 2$ ,  $m$  edges are “glued” onto an existing  $(m - 1)$ -simplex  $\Delta_{m-1}$  to form an  $m$ -simplex  $\Delta_m$ . If  $n = 3$ , the  $m$ -simplex  $\Delta_m$  is built by “glueing”  $m$  edges to an existing  $(m - 1)$ -simplex  $\Delta_{m-1}$  and a vertex.

More concretely, this means that the move  $1_1$  adds an edge whose vertices have both valence 1. The move  $2_1$  adds an edge such that one vertex of the edge has valence 1 and the other vertex has valence greater than 1. The  $3_1$  move adds an edge between two existing vertices.

I also introduce a fourth move, called  $4_1$ . It adds an edge between two vertices that are linked to a common vertex, but are not linked directly. These moves are redundant in the sense that they are equivalent to a subset of the  $3_1$  moves. The  $4_1$  moves are nevertheless important, since the explicit proposal of such moves makes the algorithm far more efficient in finding minimum energy configuration. They appear to facilitate the growth of 2-simplices and surfaces.

In the case  $m = 2$ , we have, in analogy to  $2_1$ , the  $2_2$  move which “glues” two edges  $a$  and  $b$  to an existing edge  $c$  such that  $a, b, c$  form a 2-simplex. The vertex shared by  $a$  and  $b$  has

---

<sup>4</sup> It is another question whether this sampling is also unbiased, i.e. representative of the low-temperature equilibrium. This will be discussed in section V.

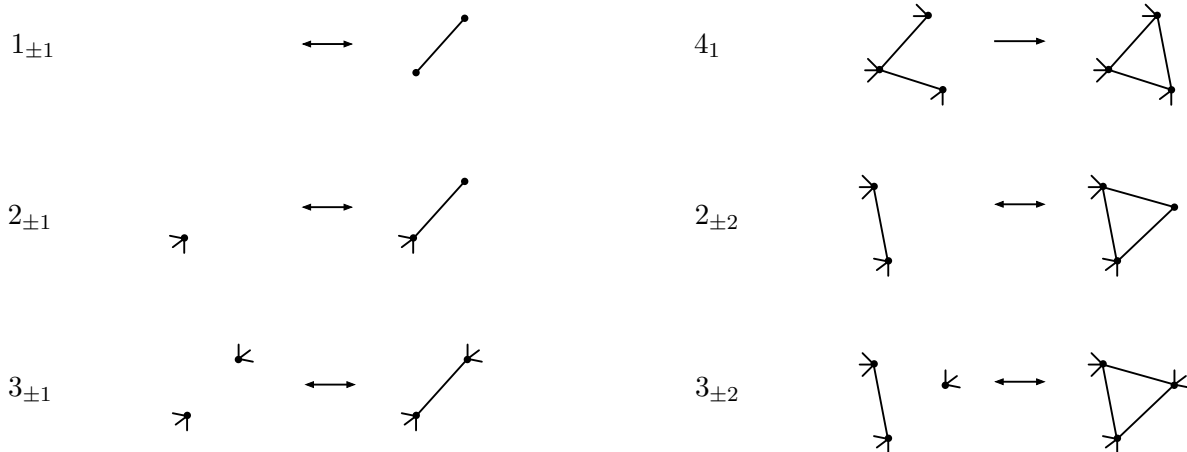


Figure 2: List of moves from which Monte Carlo moves are built.

valence 2. The move  $3_2$  does the same as  $2_2$  except that the vertex common to  $a$  and  $b$  has valence greater than 2 (i.e. one end of  $a$  and  $b$  is “glued” to an existing vertex of the graph). Like the  $4_1$  move, the  $2_1$  and  $2_2$  move are not needed for ergodicity, but they enhance the algorithm’s efficiency at low temperature.

In principle, one could also define a  $1_2$  move that adds a disconnected 2–simplex. However, I found it easier to omit this move in the algorithm. Since the edge number is conserved,  $1_2$  would have to be accompanied by two moves of  $m = -1$ , which would require additional program code.

The moves  $n_m$  with negative  $m$  are defined as the inverses of those with  $m > 0$ . Altogether we have the following set of basic moves<sup>5</sup>:

$$\{1_{\pm 1}, 2_{\pm 1}, 3_{\pm 1}, 4_1, 2_{\pm 2}, 3_{\pm 2}\}$$

Each of the Monte Carlo moves is given by a sequence of moves  $(n_{-m}, n'_m)$ ,  $m > 0$ , where  $n_{-m}$  and  $n'_m$  are taken from the previous set.

## B. Trial probabilities and detailed balance

Next I describe the way Monte Carlo moves are proposed. The resulting proposal (or trial) probabilities are generally not symmetric w.r.t. inversion of the move. Therefore, to ensure detailed balance, we need to include trial probabilities when determining the acceptance probability.

The trial probability for the Monte Carlo move  $(n_{-m}, n'_m)$  is given by

$$P_t(n_{-m}, n'_m) = P_t(n_{-m})P_t(n'_m), \quad (9)$$

where  $P_t(n_{-m})$  and  $P_t(n'_m)$  are the trial probabilities for the subtraction and subsequent addition of edges.

<sup>5</sup> We do not need  $4_{-1}$ , since 2–simplices are easily destructed by  $3_{-1}$ .

For the subtraction move  $n_{-m}$ ,  $m > 0$ , the selection proceeds as follows. There is a probability  $P_m$  of choosing  $m = 1$  or  $m = 2$  that is weighted in a specific manner by the number of existing simplices. Then, we have a probability  $P_{\Delta_m}$  for choosing the  $m$ -simplex  $\Delta_m$  on which the move operates. This simplex is chosen randomly from the set of  $m$ -simplices, so

$$P_{\Delta_m} = \frac{1}{N_{\Delta_m}}. \quad (10)$$

Finally, one has to select the type  $n$  of the move. The probability  $P_n$  for this is 1 in all cases except for  $3_{-2}$ , where it is  $P_3 = 1/3$ , since there are three ways of removing two edges from a given 2-simplex. The overall trial probability for the subtraction move  $n_{-m}$  is

$$P_t(n_{-m}) = P_m P_{\Delta_m} P_n. \quad (11)$$

In the case of the additive move, we do not have to choose  $m$ , since it is fixed by the previous removal of edges. The choice of type  $n'$  is based on a certain weighting  $P_{n'}$  whose details we omit. The non-trivial part is the probability  $P_{\text{rec}}(n'_m)$  for selecting the simplices that serve as “receptors” for the edges to be added. For moves of type 1,  $P_{\text{rec}}(1_m) = 1$ . For  $n' = 2$ , we have

$$P_{\text{rec}}(2_m) = P_{\Delta_{m-1}} = \frac{1}{N_{\Delta_{m-1}}}, \quad (12)$$

where  $P_{\Delta_{m-1}}$  is the likelihood of picking one of the  $(m-1)$ -simplices at random. For  $n' = 3$ , one has to choose both an  $(m-1)$ -simplex and a vertex, therefore

$$P_{\text{rec}}(3_m) = P_{\Delta_{m-1}} P_v = \frac{1}{N_{\Delta_{m-1}} N_v}. \quad (13)$$

The total trial probability for  $n'_m$  is

$$P_t(n'_m) = P_{n'} P_{\text{rec}}(n'_m). \quad (14)$$

An exception to this rule occurs when we deal with a move that is both  $3_1$  and  $4_1$ . In this case, we have

$$P_t(3_1) \equiv P_t(4_1) = P_3 P_{\text{rec}}(3_1) + P_4 P_{\text{rec}}(4_1), \quad (15)$$

where  $P_{\text{rec}}(3_1)$  is given as before and  $P_{\text{rec}}(4_1)$  is the likelihood of proposing the receptors of the  $4_1$  move. The latter are determined by first choosing a vertex  $v_c$  that I call the “center” vertex and then vertices  $v_1$  and  $v_2$  that are linked to  $v_c$ , but not linked to each other (see Fig. 2). Thus, the likelihood for a given pair  $(v_1, v_2)$  can be written as

$$P_{\text{rec}}(4_1) = \frac{1}{N_v} \sum_{v_c} \frac{1}{N_{v_c}}. \quad (16)$$

Here, the sum extends over all center vertices  $v_c$  compatible with the pair  $(v_1, v_2)$ , while  $N_{v_c}$  is the number of *all* pairs  $(v_1, v_2)$  for which  $v_c$  is a center vertex.

Once the trial probabilities are determined, we can evaluate the acceptance probability  $P_a(n_{-m}, n'_m)$  via

$$P_a(n_{-m}, n'_m) = \min \left\{ 1, \frac{P_t(n'_{-m}, n_m)}{P_t(n_{-m}, n'_m)} e^{-(E'-E)/T} \right\}. \quad (17)$$

$E$  and  $E'$  denote the energy before and after the move.

|             | $T$         | $\Delta t_{\text{eq}}$ | $t_{\text{MC}}$ |
|-------------|-------------|------------------------|-----------------|
| $N_e = 45$  | 0.5 – 2.0   | $7 \cdot 10^6$         | $7 \cdot 10^8$  |
|             | 2.25 – 6.75 | $1 \cdot 10^6$         | $1 \cdot 10^8$  |
| $N_e = 90$  | 0.5 – 2.0   | $7 \cdot 10^6$         | $7 \cdot 10^8$  |
|             | 2.25 – 6.75 | $1 \cdot 10^6$         | $1 \cdot 10^8$  |
| $N_e = 180$ | 0.5 – 1.5   | $2 \cdot 10^7$         | $2 \cdot 10^9$  |
|             | 1.625 – 2.5 | $7 \cdot 10^6$         | $7 \cdot 10^8$  |
|             | 2.75 – 6.75 | $1 \cdot 10^6$         | $1 \cdot 10^8$  |

Table I: Equilibration times and total number of Monte Carlo steps.

#### IV. RESULTS OF THE SIMULATION

In this section, I present the results of the simulation. Measurements were done for three sizes of the system,  $N_e = 45, 90$  and  $180$ , and for a range of temperatures from  $T = 0.5$  to  $T = 6.75$ . I begin with the estimates for equilibration times (the next subsection). Then, in subsection IV B, I describe the results for the two main observables, the energy  $E$  and the observable  $M$  (defined in eq. (6)), and the quantities derived from them, the specific heat per edge  $c$  and the susceptibility  $\chi$  associated to  $M$  (see eq. (8)). In subsection IV C, the low-temperature regime is investigated in more detail with regard to topology, curvature and defects. In section V, I will discuss the issue of equilibrium at low temperature and caveats entailed by it.

##### A. Equilibration times

Figure 3 contains examples of plots used to estimate the equilibration times for different temperatures  $T$  and sizes  $N_e$  of the system. The plots show data from preparatory simulations that measured the energy per edge  $\epsilon = E/N_e$  and the observable  $m = M/N_e$  for a duration of  $t = 2 \cdot 10^7$  Monte Carlo steps. The starting configuration is a graph of  $N_e$  disconnected edges

It should be noted how the characteristics of the plots change as we go from low to higher temperatures. The plot is very autocorrelated for  $T = 0.5$ , becomes less correlated and more fluctuating at  $T = 1.125$ , and turns into strong fluctuations with little autocorrelation at  $T = 1.5$ .

Based on these plots and similar ones for other temperatures and edge numbers, I adopted a set of equilibration times  $\Delta t_{\text{eq}}$  for the main simulation which are listed in table I. The total number of Monte Carlo steps  $t_{\text{MC}}$  is taken to be  $100\Delta t_{\text{eq}}$  in each case.



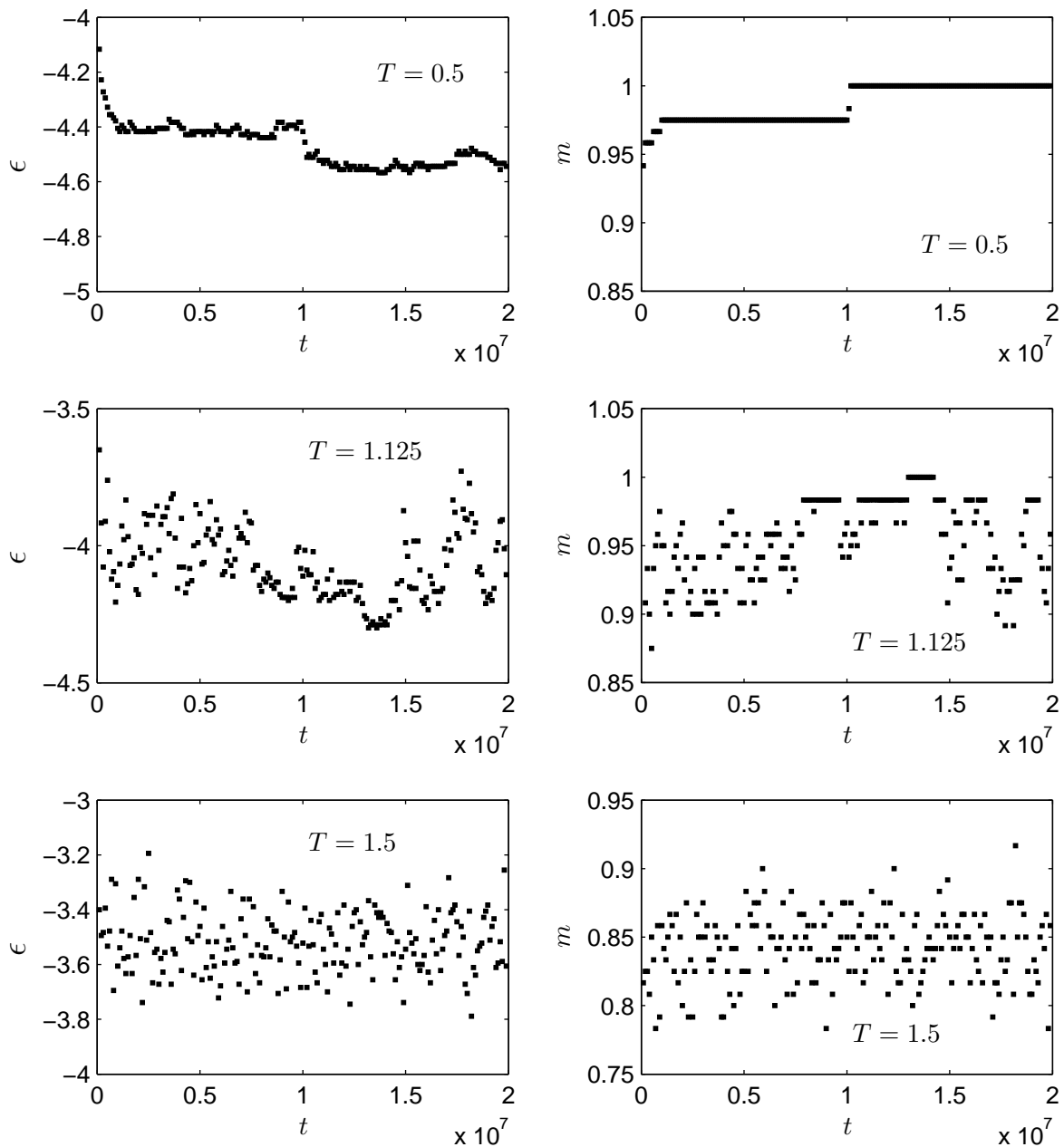


Figure 3: Examples of plots that were used to estimate equilibration times  $t_{\text{eq}}$ : energy per edge  $\epsilon$  and  $m$  versus simulation time  $t$  for  $N_e = 180$  edges.

### B. Evidence for a phase transition?

Figure 4 displays the simulation results for the energy per edge  $\epsilon$  and the observable  $m$ . Here and in the following error bars are omitted whenever they are smaller than the symbols of the data points<sup>6</sup> At sufficiently low temperature  $m$  reaches the value 1 and, up to conical

<sup>6</sup> Correlation times and error estimates will be addressed in section V.

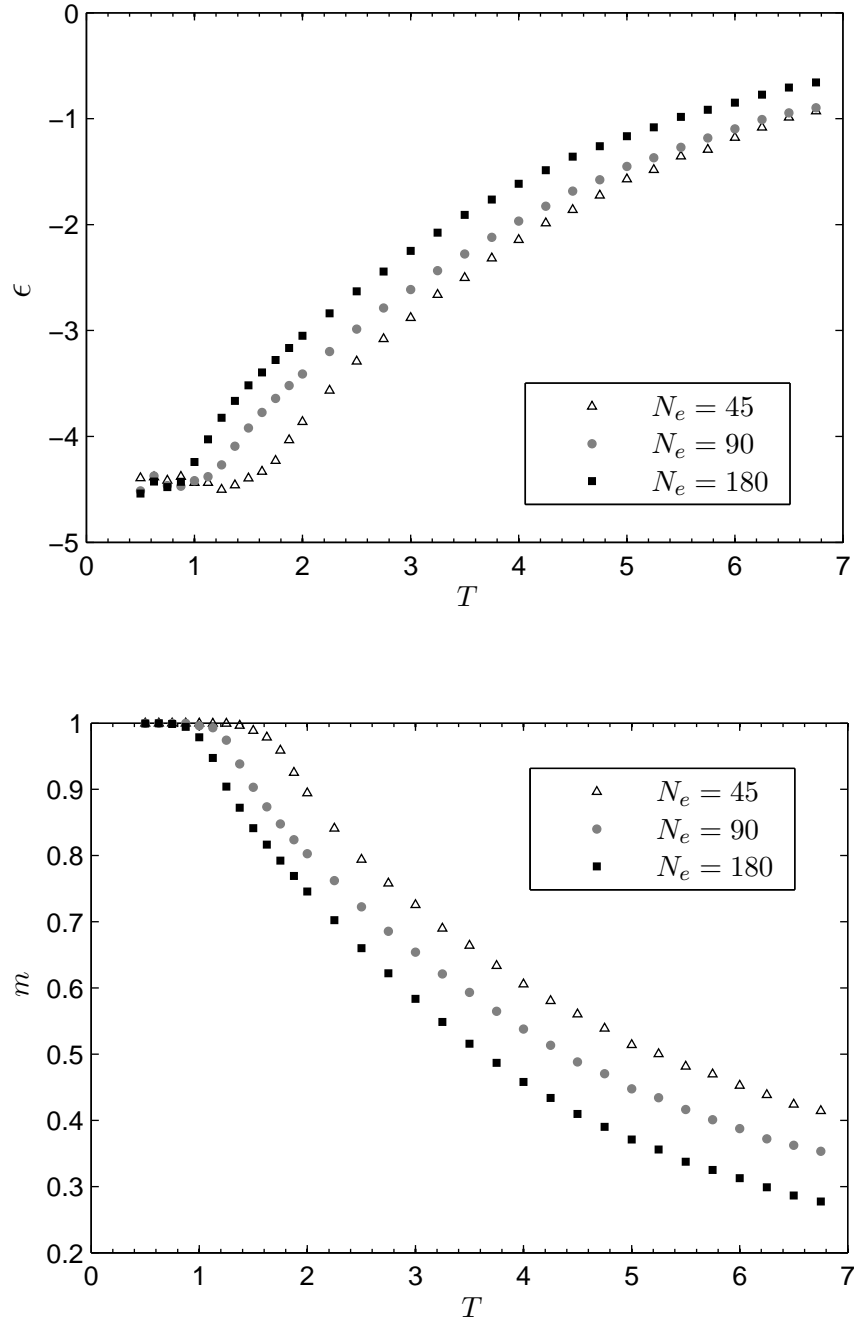
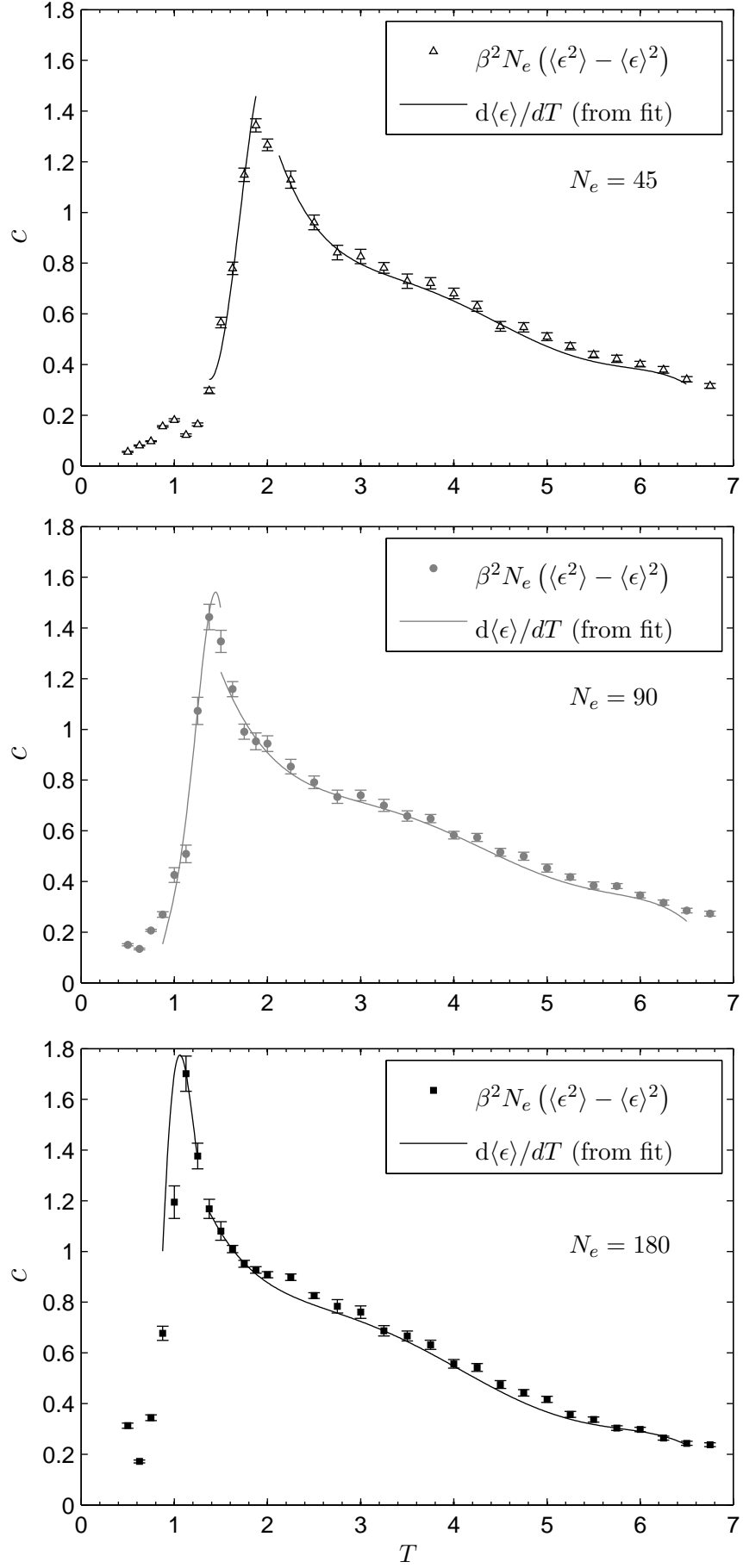


Figure 4: Energy per edge  $\epsilon$  and  $m$  versus temperature  $T$  for edge number  $N_e = 45, 90$  and  $180$ .

singularities, the average graph is given by a surface without boundary. This confirms the expectations expressed in the previous section. The attainment of  $m = 1$  goes along with the energy per edge reaching its bottom value. (Curiously, for  $N_e = 45$ , the energy rises again slightly as  $T$  decreases further. This might be related to incomplete equilibration at low temperatures, see subsec. V). The transition temperature, where  $m = 1$  sets in, decreases as  $N_e$  increases.

That something interesting happens when  $m$  becomes 1 is also suggested by the results

Figure 5: Specific heat per edge  $c$  versus temperature  $T$  for  $N_e = 45, 90$  and  $180$ .

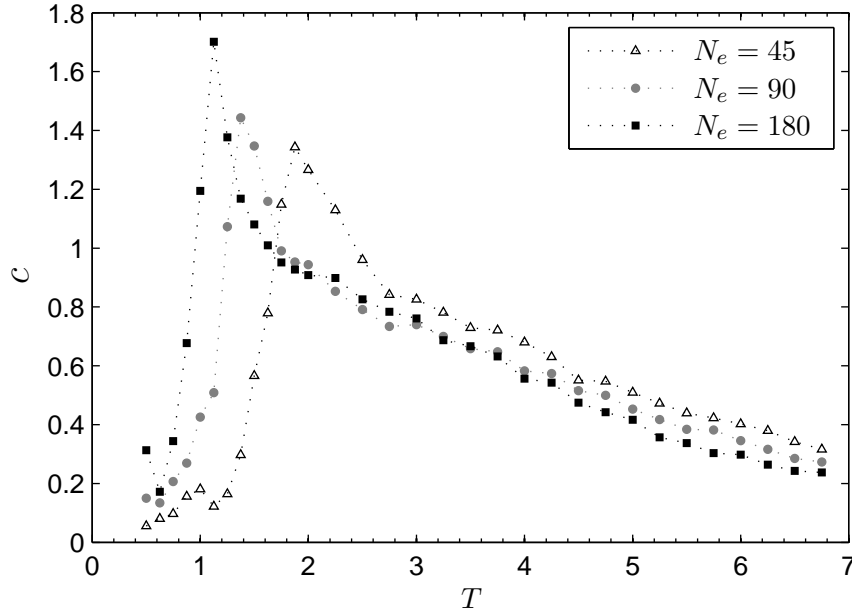


Figure 6: Specific heat per edge  $c$  versus temperature  $T$ .

for the specific heat, shown in Fig. 5. The specific heat can, in principle, be determined in two ways; from the variance,

$$c = \beta^2 N_e (\langle \epsilon^2 \rangle - \langle \epsilon \rangle^2) , \quad (18)$$

or from the temperature derivative of the average energy per edge  $\langle \epsilon \rangle$ :

$$c = d\langle \epsilon \rangle / dT \quad (19)$$

In theory these formulas should give the same value, and the same should hold for measurements in the simulation, if the sampling is representative of the equilibrium.

In Fig. 5 the symbols represent the values of  $c$  obtained via formula (18). The errors are estimated by the blocking method. The continuous lines, on the other hand, come from fitting polynomials to the  $\epsilon$ - $T$  plots in Fig. 4 and then taking the derivative with respect to  $T$ . We see that in the temperature range of the fits there is relatively good agreement between the two methods, thus suggesting that the simulation is equilibrated.

The most notable feature of the plots are the peaks which reside near the temperature where  $m$  reaches 1. For  $N_e = 45, 90$  and  $180$  the peaks lie at  $T = 1.875, 1.375$  and  $1.125$  respectively<sup>7</sup>. For easier comparison, the curves for different  $N_e$  are plotted together in Fig. 6. The dotted line was added for clarity and connects the points by straight lines.

This plot should be compared with Fig. 7, which was obtained by taking the discrete forward derivative of the points in the  $m$ - $T$  plot. The peaks of  $|\frac{\Delta m}{\Delta T}|$  are slightly shifted relative to those of  $c$ . This may be an artifact resulting from the use of the forward derivative.

<sup>7</sup> It is not an accident that these values are close to 1. When choosing the couplings in the Hamiltonian, I tuned them to the onset of surface formation, while  $T$  was set to 1.

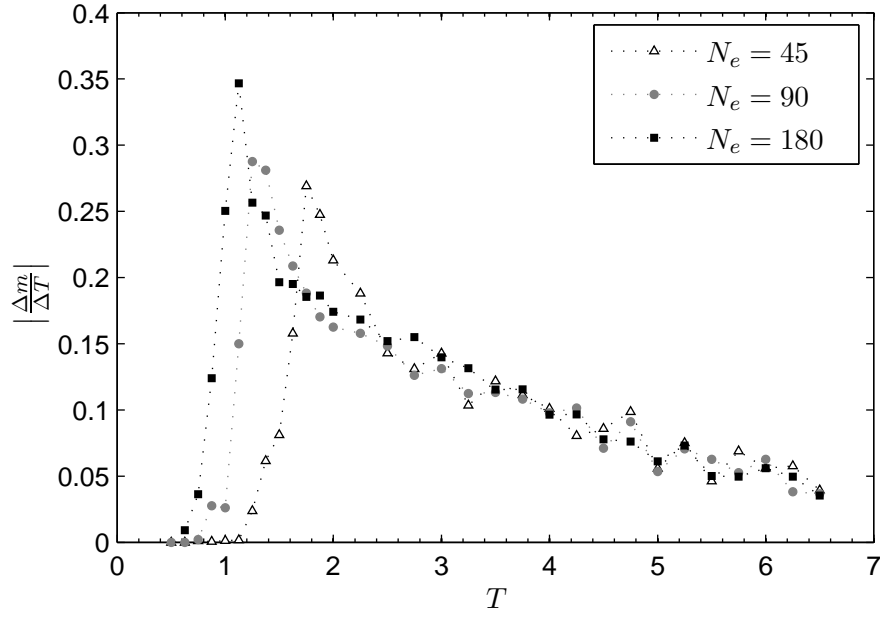


Figure 7: Forward derivative of measured values of  $m$  with respect to temperature  $T$ .

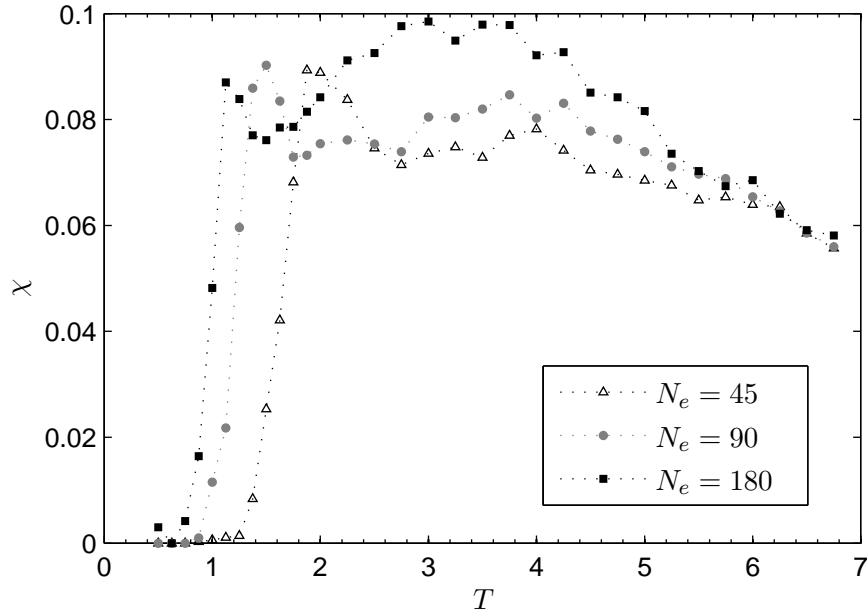


Figure 8: Susceptibility  $\chi$  versus temperature  $T$ .

Figure 8 shows the results for the susceptibility  $\chi$  defined in eq. (8).  $\chi$  exhibits a sharp increase at the transition temperature. Unlike for a ferromagnet, there is no peak, however, since  $\chi$  stays more or less constant, as  $T$  is further increased.

The salient properties of our data can be summarized as follows. Below a transition temperature  $T_{\text{trans}}$  the surface observable  $m$  is constant and equals 1. At the temperature  $T_{\text{trans}}$ ,

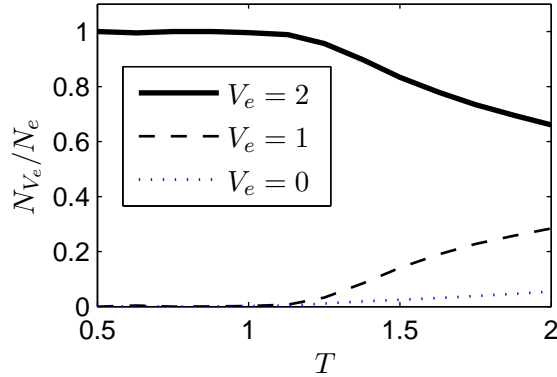


Figure 9: The fraction of edges with valence  $V_e$  versus the temperature  $T$  for  $N_e = 90$ .

$m$  starts to decrease. The rate of this decrease grows as  $N_e$  increases. That is, the kink in the  $m$ - $T$  curve becomes more pronounced as the system becomes larger. At the transition temperature  $T_{\text{trans}}$ , we also see a peak in the specific heat  $c$  whose amplitude increases with system size. The peak in  $c$  is accompanied by a notable increase in the time  $\Delta t_{\text{eq}}$  needed to equilibrate the system. A further indicator is the “susceptibility”  $\chi$  which shows a sharp rise at  $T = T_{\text{trans}}$ .

One can infer from this that for  $T < T_{\text{trans}}$  the system is characterized by surface-like graphs for which  $m = 1$ . For  $T > T_{\text{trans}}$ , these surfaces are replaced by more general graphs with  $m < 1$ . The observable  $m$  serves as a parameter to distinguish these two regimes.

The  $T$ -dependence of the specific heat is similar to what is found in more conventional systems with phase transitions. It should be noted, however, that the peak of the specific heat shifts to lower temperatures, as the system size increases. Thus, it is possible that the transition temperature  $T_{\text{trans}}$  goes to zero in the infinite size limit. Given that I have measured three sizes up to  $N_e = 180$  so far, it is premature to conclude whether this is the case or not. That is, one cannot tell at this stage if the system exhibits a phase transition at zero  $T$  or at finite  $T$ . Further remarks on this will be made in the conclusion of the paper.

### C. Surface properties

This subsection deals in more detail with the surface states found at low temperature. What kind of surfaces appear? What defects do they have? And how do they change when  $T$  is increased?

To answer these questions I conducted two additional sets of simulations. The first kind of simulation was aimed at showing more precisely how the valence of edges evolves as the temperature is raised above the transition temperature. This led to the plots in Fig. 9. For  $T < T_{\text{trans}}$  almost all edges have valence  $V_e = 2$ . At  $T = T_{\text{trans}}$  the fraction of these edges starts to decrease until it drops to around 66 percent at  $T = 2.0$ . In parallel the fraction of boundary edges ( $V_e = 1$ ) rises from 0 percent to about 28 percent at  $T = 2.0$ . The percentage of edges outside of triangles ( $V_e = 0$ ) increases as well and reaches 5 percent. It is clear from this that at  $T = 2.0$  the graphs must have lost most of its resemblance with a surface, since a considerable fraction of edges form boundaries of triangles.

|                        |                 |                 |                  |  |
|------------------------|-----------------|-----------------|------------------|--|
| $T$                    | 0.625           | 2.0             | $N_v$            | # of vertices                            |
| $N_{V_e=0}/N_e$        | $0.00 \pm 0.00$ | $0.09 \pm 0.01$ | $N_e$            | # of edges                               |
| $N_{\text{con}}/N_v$   | $0.08 \pm 0.01$ | $0.40 \pm 0.02$ | $N_{V_e=0}$      | # of edges with valence $V_e = 0$        |
| $N_{cc}$               | $1.2 \pm 0.1$   | $2.6 \pm 0.3$   | $N_{\text{con}}$ | # of conical singularities               |
| $V_v$                  | $6.7 \pm 0.1$   | $5.3 \pm 0.1$   | $N_{cc}$         | # of connected components of surface     |
| $R$                    | $-0.8 \pm 0.1$  | $3.0 \pm 0.3$   | $V_v$            | (average) valence of vertices            |
| $N_{be}^{lc}/N_e^{lc}$ | $0.00 \pm 0.00$ | $0.36 \pm 0.01$ | $R$              | (average) Ricci scalar                   |
| orientability          | $0.00 \pm 0.00$ | $0.07 \pm 0.01$ | $N_e^{lc}$       | # of edges in largest component          |
| $\chi_{\text{Euler}}$  | $-6.1 \pm 0.4$  | $-4.8 \pm 0.4$  | $N_{be}^{lc}$    | # of boundary edges in largest component |

Table II: Surface properties for edge number  $N_e = 180$  and temperatures  $T = 0.625$  and  $T = 2.0$ . The table consists of three sections which refer to the graph, the surface (defined by the reduced graph) and the largest component in the surface.

The second type of simulation concerned defects, topology and curvature. The measurements proceeded in three steps. First, the conical singularities and the edges with zero valence are determined and counted. Then, these defects are removed, so that one obtains a reduced graph that is equivalent to a triangulation of a surface. This reduction to a surface is needed in order to have a well-defined notion of topology. In the third step, we measure various quantities related to topology, boundary size and curvature of the surface.

The curvature is obtained by interpreting the triangulation as a piecewise-linear manifold whose edges have length 1. The deficit angle at a vertex is given by

$$\delta_v = 2\pi - V_v\pi/3 \quad (20)$$

and the Ricci scalar is defined by

$$R_v = \frac{2\delta_v}{A_v}. \quad (21)$$

Here,  $A_v = V_v A/3$  is the area associated to the vertex, and  $A = \sqrt{3}/4$  is the area of the triangles of the triangulation (see e.g. [26]).

Since these measurements involve a change in the graph (and saving graphs was not implemented in the code), I ran the simulation differently from the previous ones. Instead of a sequence start  $\rightarrow$  equilibrate  $\rightarrow$  measure  $\rightarrow$  wait  $\rightarrow$  measure  $\dots$ , I used a schedule that restarts the simulation after each measurement:

start  $\rightarrow$  anneal  $\rightarrow$  equilibrate  $\rightarrow$  measure  
 $\rightarrow$  restart  $\rightarrow$  anneal  $\rightarrow$  equilibrate  $\rightarrow$  measure  $\dots$

A similar simulation schedule will also play a role in the next section, where I discuss equilibration at low temperature.

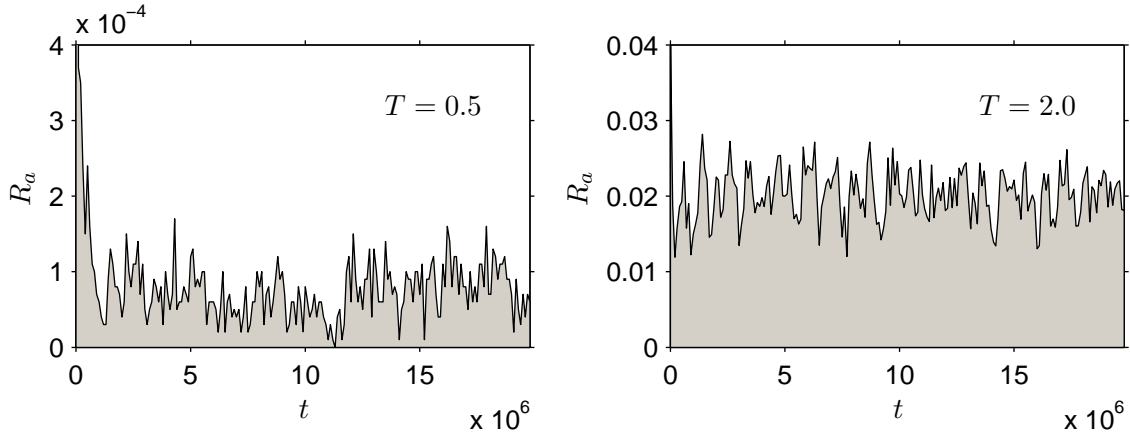


Figure 10: Acceptance rate  $R_a$  versus step number  $t$  for  $T = 0.5$  and  $T = 2.0$ .

The results are given in table II. I ran the simulation for  $T = 0.625$  and  $T = 2.0$  to compare the graph properties below and above the critical temperature. At low temperature, the graph contains no edges with valence  $V_e = 0$ . Eight percent of the vertices come with conical singularities. The typical surface consists of a single connected component with moderate curvature. The largest component of the surface has no boundary, it is non-orientable and on average given by a connected sum of 8 real projective spaces. (Recall that a non-orientable surface with Euler characteristic  $\chi_{\text{Euler}} = 2 - k$  is a connected sum of  $k$  real projective planes.)

At the temperature  $T = 2.0$  above the transition point, the number of edges outside triangles is 9 times larger than in the surface regime, and the fraction of conical singularities reaches 40 percent. While we can still define a reduced graph and hence a surface, it is no longer a surface in the usual sense of the word. In the largest component, 30 to 40 percent of the edges are boundary edges.

Let me add that I also tried to measure the spectral dimension of the graphs. This attempt failed, however. When measuring the return probability of diffusion, there is typically a window in the diffusion time that can be used to determine the spectral dimension. For diffusion times outside this interval the measurement is hampered by discretization and finite volume effects. In the present case, the system size appears to be so small ( $N_e \leq 180$ ) that discrete and finite volume effects overlap, and no clear signal of the spectral dimension is visible.

## V. SUBTLETIES AT LOW TEMPERATURE

The simulation of systems with complex energy structure and many degeneracies can pose considerable challenges, especially at low temperatures. Well-known examples for this are systems with quenched disorder such as spin-glasses and random field systems (see e.g. [20–22]). The simulation may get trapped in certain configurations, and never find the bottleneck to exit and enter other regions. It may sample some of the ground states, but leave out others, and thus create biased results that are not representative of the true equilibrium.



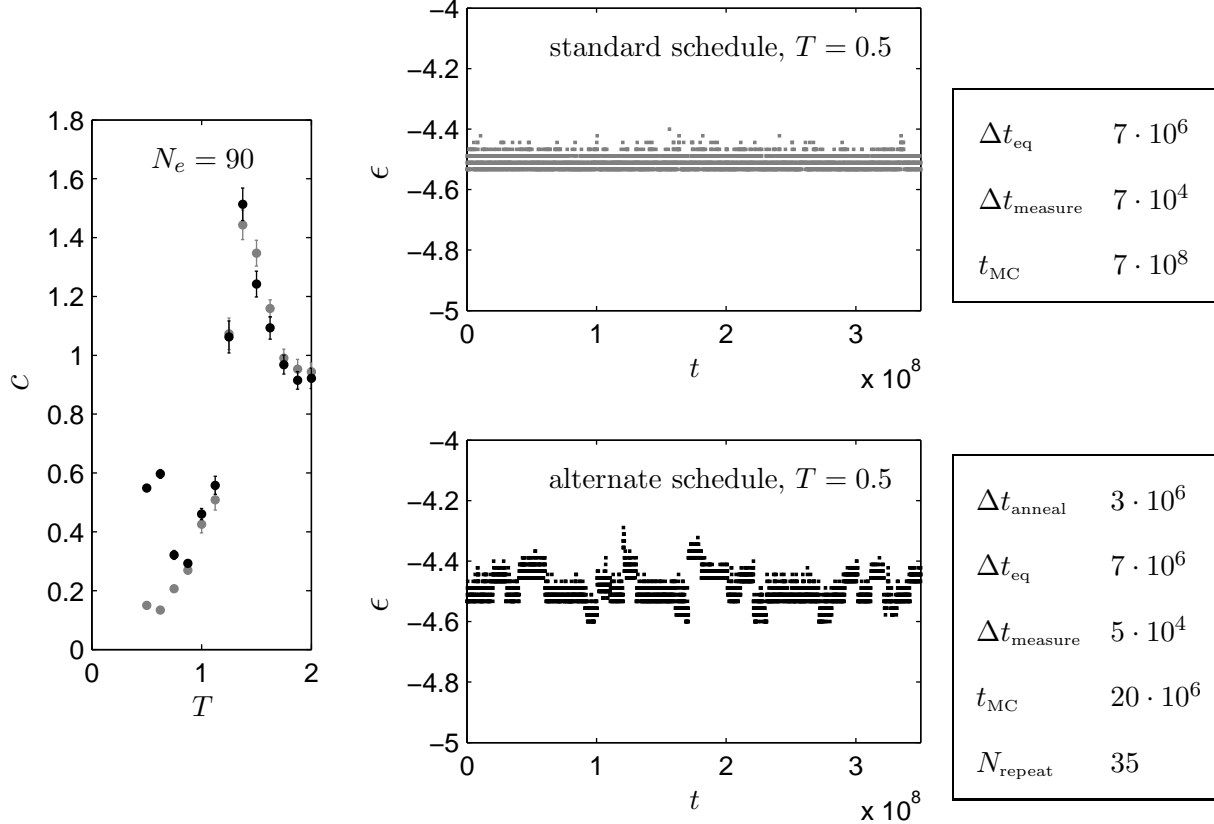


Figure 11: Comparison of the standard and alternate simulation schedule: on the left, specific heat  $c$  versus temperature  $T$  for standard schedule (grey) and modified schedule (black); in the middle, plot of  $\epsilon$  vs. simulation time  $t$ ; on the right, parameters of Monte Carlo simulation.

The ground states of the present model form a very special subset of the entire configuration space. Therefore, it is not far-fetched to imagine that similar difficulties could occur here. A first indication of this problem can be seen in the very small acceptance rates at low temperature. While the acceptance is already low, in general, it drops to values below  $10^{-3}$  as we reach  $T = 0.5$  (see Fig. 10). Real-time visualization with the Ubigraph software revealed that at this temperature the accepted changes are predominantly 2–2 Pachner moves—moves that are not able to change the topology of a triangulation.

The question is therefore the following. Can the simulation sample the low-energy states in a statistically correct way, or does it get stuck in a minimum energy state and stay there for the rest of the simulation? To obtain more information about this, I repeated some of the previous simulations with a different schedule. In this new schedule, a phase of annealing and equilibration is followed by a sequence of measurements, then the simulation restarts and the whole process is repeated. This procedure may yield a better sampling of ground states and shorten the time during which the algorithm is trapped. The precise parameters of the original and modified schedule are indicated in Fig. 11. During annealing the temperature starts at  $T = 4.0$  and drops gradually to the target temperature.

The two types of simulations agree reasonably well for  $T \geq 1.0$ . For the lowest temperatures, however, the alternate schedule leads to a much higher value of the specific heat. The

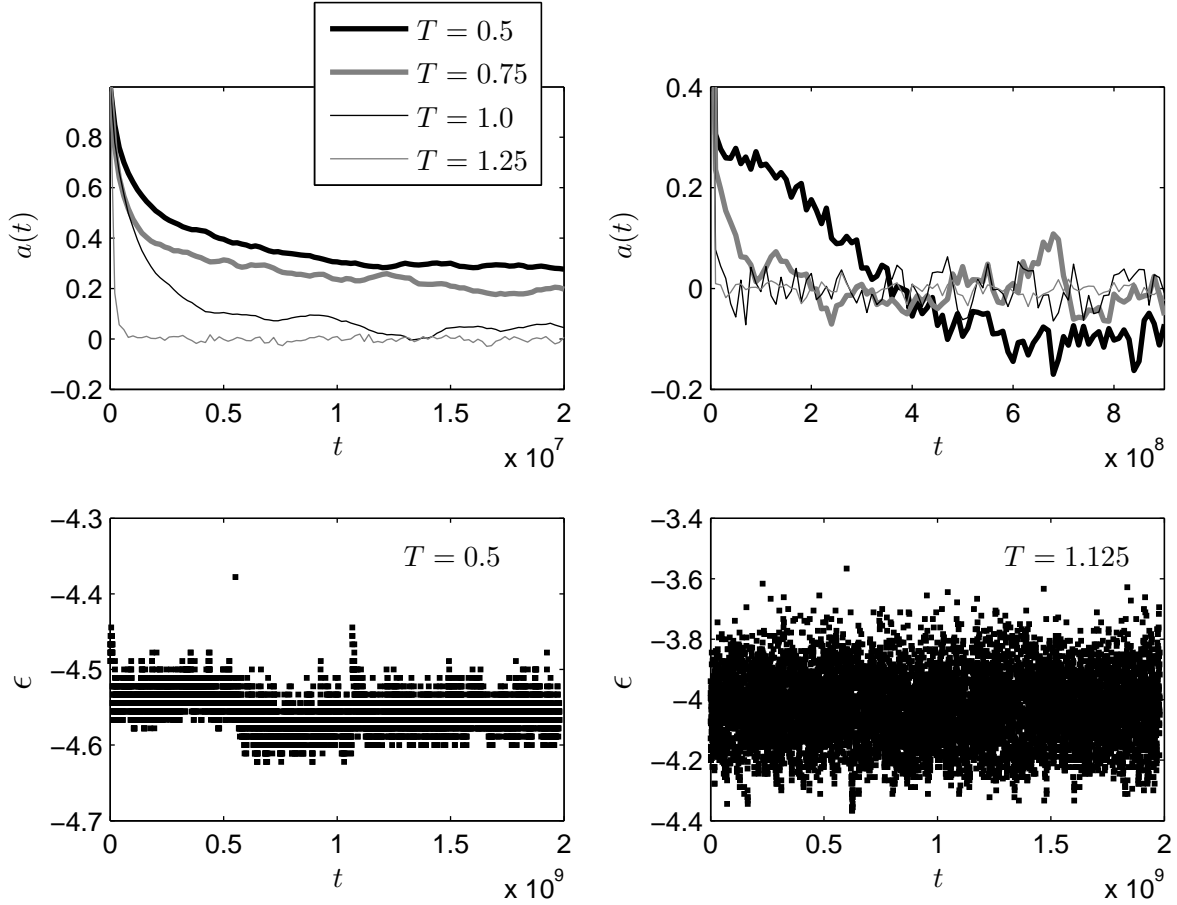


Figure 12: Autocorrelation function  $a(t)$  of  $\epsilon$  for different temperatures and  $N_e = 180$ .

reason for this difference becomes clear when we inspect the measured data for the energy per edge (see Fig. 11). In the standard case, the fluctuations exhibit a fixed pattern for the length of the entire simulation. In the alternate case, the same kind of pattern appears, however, only for the duration of a single measurement period. At the beginning of the following measurement sequence, the pattern jumps to a new energy and remains there until the next restart.

This suggests the following interpretation. The standard schedule gets stuck in one set of states and stays there for the rest of the simulation. The alternate schedule gets trapped as well, but only for a short period and each time for a different energy. This sampling of different states results in a too large variance and hence in a wrong value for the specific heat. Within this sample, however, there are also states that have lower energy than the states found by the conventional scheme. Thus, there is something wrong and right in both methods. The original simulation yields the correct specific heat, but the measured energy may be too high, if the algorithm freezes in a set of states above the true ground state.

The last point to be addressed is the autocorrelation of our data (see Fig. 12). For temperatures greater than  $T_{\text{trans}}$ , the autocorrelation drops exponentially to zero and I determined corresponding correlation times  $\Delta t_{\text{cor}}$  for the error analysis. For  $T < T_{\text{trans}}$ , on the other hand, the data are, in many cases, autocorrelated on time scales of the order of  $t_{\text{MC}}$ ,

so I would not be able to correct this other than by going to much larger simulation times. The plots show furthermore that my estimates for the equilibration time were too optimistic at low temperatures.

## VI. CONCLUSION

Let me summarize the results. I have defined a graph model that produces “space from no space”. Two-dimensional triangulations (space) arise as ground states from a much larger set of configurations (no space). To measure the extent to which a graph is a surface I introduced an observable called  $m$ . Monte Carlo simulations show that below a transition temperature  $T_{\text{trans}}$  the observable  $m$  is close or equal to 1, and the graphs form triangulations of surfaces<sup>8</sup>. For temperatures  $T > T_{\text{trans}}$ , one has  $m < 1$  and the surfaces are replaced by more general graphs. More detailed measurements reveal that the surfaces are typically connected and non-orientable. As we go above the transition temperature, the graphs lose the surface structure, since the number of defects increases and many of the edges become boundaries of triangles.

The temperature dependence of  $m$  and of the specific heat  $c$  suggest that there is a phase transition between the regime with and without surfaces. However, the transition temperature  $T_{\text{trans}}$  drifts, as the system size is increased, so it is possible that  $T_{\text{trans}}$  goes to zero in the infinite-size limit. In this case, there would be no phase transition at finite temperature, and one would instead speak of a *zero temperature phase transition*. Since the system was only simulated for very few and small sizes, it is too early to tell which scenario is realized.

What are future directions for this work? Obviously, one should try to extend the model to larger sizes and higher, more realistic dimensions. The key technical question in this will be whether one is able to make the algorithm efficient enough to sustain equilibrium at low temperature. It may be necessary to invent more sophisticated simulation schedules in order to deal with larger edge numbers and higher-dimensional simplices. Another remedy could be to use a different Hamiltonian that is more “flexible” in its choice of ground states. By this I mean that ground states would not only be given by graphs that are literally 2d triangulations, but also by more general graphs that are effectively 2-dimensional (e.g. in the spectral sense). Perhaps one could define a “spectral Hamiltonian” that achieves this.

Furthermore, one should determine conclusively whether there is a phase transition, and if it is at finite or zero temperature (in the infinite-size limit). A phase transition at finite temperature is desirable in the sense that it would make the behaviour near the transition universal and reduce the amount of fine-tuning needed to achieve this state. In the case of a zero temperature phase transition, the dimensionless couplings would have to be sent to infinity as the system size goes to infinity in order to maintain a transition at finite  $T$ .

Since the paper focused on the technical aspects, I would like to conclude with a number of conceptual remarks. An obvious question pertains to the role of time. If this is a statistical model of space, there must be a time with respect to which the system equilibrates. If that is the case, it would seem that, in the model’s world, time is of a different nature than space, since space can dissolve, while there is always time for the system to thermalize.

Let me give a possible interpretation of the model that clarifies this point. Imagine that

---

<sup>8</sup> modulo conical singularities

we had a consistent quantum theory of gravity that describes spacetime as being built from elementary cells or building blocks. Assume also that from a canonical point of view this spacetime corresponds to blocks or “atoms” of space that evolve in a discrete, fluctuating time. If the theory is a viable candidate theory of quantum gravity, there should be a regime where classical continuum spacetime is recovered from the collective properties of these atoms. Like in conventional quantum theories, one might furthermore expect that there is a statistical approximation of the theory, where the 4d path integral is replaced by a statistical sum over 3d configurations. Our model could be regarded as such a statistical approximation to a quantum theory of spacetime (in this case 3d spacetime). The edges of the graphs are the atoms of space and their interactions are encoded by the Hamiltonian<sup>9</sup>.

This line of thought suggests also a connection with group field theory and loop quantum gravity. The quanta of these theories are triangles and tetrahedra and interact to form pseudo-manifolds [27–29]. If we were able to develop a statistical theory of group field theory and loop quantum gravity, the resulting models may have a similar structure as the model defined here<sup>10</sup>.

Apart from this, our system could be also useful as a concrete and simple toy model that helps to imagine what a physics beyond spacetime could be; a physics, that is, in which spacetime is no longer absolute and instead only a special state among other states of the system. This dethroning of spacetime is, in my view, a logical continuation of the development of theoretical physics. It is also a radical step that challenges accustomed ways of thinking about physics. Let me highlight this by describing three thought experiments that could be simulated with our model.

There is a 1d version of the Hamiltonian that results in the formation of 1d chains at low temperature. Imagine that we combine the 1d Hamiltonian with the 2d Hamiltonian used in this paper. Then, one could vary the relative strength of the 1d and 2d couplings and observe transitions between a 1-dimensional and 2-dimensional phase of the system.

As a second example, consider the surface regime of the model and suppose that we encode a picture on the surface by affixing additional labels to edges. Next let us raise the temperature until the surface disappears completely. Then, we go back to the original temperature and a surface will form again. The picture, however, will be scrambled, since the arrangement of edges is completely reshuffled. One can view this as an instance of spontaneous symmetry breaking.

Another version of this argument explains nicely the intimate connection between space and Hamiltonian (or spacetime and Lagrangian). Suppose that we extend the system by adding spins to the triangles and let these spins interact by the usual nearest-neighbour Hamiltonian. Assume furthermore that the energy scale of the spin field is small enough to not affect the dynamics of the graphs. At low enough temperatures, the graphs freeze in a surface state and the system becomes effectively an Ising model on a fixed lattice. Note, however, that it is the graph that determines which spin neighbours which other spin and hence which spins couple to each other. In this sense, the graph (or space) is part of the spin system’s coupling constants. By the same token, if space is a variable, the coupling constants are variables as well.

---

<sup>9</sup> Clearly, this is just a heuristic consideration and leaves out many questions. What effect would fluctuations of time have? How can Lorentz invariance be maintained?

<sup>10</sup> See [30] for another possible link between loop quantum gravity and statistical physics.

## Acknowledgments

I thank Leo Kadanoff and Seth Major for helpful discussions. I also thank Ky Le for assistance in installing the Ubigraph package. This work was made possible by the facilities of the Shared Hierarchical Academic Research Computing Network (SHARC-NET:www.sharcnet.ca) and Compute/Calcul Canada. Research at Perimeter Institute is supported by the Government of Canada through Industry Canada and by the Province of Ontario through the Ministry of Research & Innovation.

- 
- [1] N. Ishibashi, H. Kawai, Y. Kitazawa, A. Tsuchiya, *A large- $N$  reduced model as superstring*, Nucl.Phys. **B498**, 467 (1997), [arXiv:hep-th/9612115].
  - [2] T. Banks, W. Fischler, S.H. Shenker and L. Susskind, *M theory as a matrix model: A conjecture*, Phys.Rev. **D55**, 5112 (1997), [arXiv:hep-th/9610043].
  - [3] H. Steinacker, *Emergent Geometry and Gravity from Matrix Models: an Introduction*, Class.Quant.Grav. **27**, 133001 (2010), [arXiv:1003.4134 [hep-th]].
  - [4] L. Smolin, *Matrix universality of gauge field and gravitational dynamics*, arXiv:0803.2926 [hep-th].
  - [5] S.A. Huggett, K.P. Tod, “An introduction to twistor theory”, London Mathematical Student Texts 4 (1994).
  - [6] R. Penrose, W. Rindler, “Spinors and Space–Time; Vol. 2, Spinor and Twistor Methods in Space–Time Geometry”, Cambridge University Press, Cambridge (1985).
  - [7] J. Ambjorn, J. Jurkiewicz, R. Loll, *Causal Dynamical Triangulations and the Quest for Quantum Gravity*, arXiv:1004.0352 [hep-th].
  - [8] J. Ambjorn, J. Jurkiewicz, R. Loll, *Quantum gravity, or the art of building spacetime*, arXiv:hep-th/0604212.
  - [9] H.W. Hamber, *Quantum Gravity on the Lattice*, Gen.Rel.Grav. **41** 817 (2009), [arXiv:0901.0964 [gr-qc]].
  - [10] T. Thiemann, “Modern canonical quantum general relativity”, Cambridge University Press, Cambridge (2007).
  - [11] C. Rovelli, “Quantum Gravity”, Cambridge University Press, Cambridge (2004).
  - [12] A. Perez, *Spin foam models for quantum gravity*, Class.Quant.Grav. **20** R43 (2003), [arXiv:gr-qc/0301113].
  - [13] T. Konopka, F. Markopoulou, L. Smolin, *Quantum graphity*, [arXiv:hep-th/0611197].
  - [14] T. Konopka, F. Markopoulou, S. Severini, *Quantum Graphity: a model of emergent locality*, Phys.Rev. **D77** 104029 (2008), [arXiv:0801.0861 [hep-th]].
  - [15] T. Konopka, *Statistical Mechanics of Graphity Models*, Phys.Rev. **D78** 044032 (2008), [arXiv:0805.2283 [hep-th]].
  - [16] T. Konopka, *Matter in Toy Dynamical Geometries*, J.Phys.Conf.Ser. **174** 012051 (2009), [arXiv:0903.4342 [gr-qc]].
  - [17] A. Hamma, F. Markopoulou, S. Lloyd, F. Caravelli, S. Severini, K. Markstrom, *A quantum Bose–Hubbard model with evolving graph as toy model for emergent spacetime*, Phys. Rev. **D81** 104032 (2010), [arXiv:0911.5075 [gr-qc]].
  - [18] F. Caravelli, F. Markopoulou, *Properties of Quantum Graphity at Low Temperature*, arXiv:1008.1340 [gr-qc].

- [19] M.E.J. Newman, G.T.Barkema, “Monte Carlo Methods in Statistical Physics”, Clarendon Press, Oxford (1999).
- [20] A.P. Young, “Spin Glasses and Random Fields”, World Scientific, 1998.
- [21] A.K. Hartmann, F. Ricci-Tersenghi, *Direct sampling of complex landscapes at low temperatures: the three-dimensional +/-J Ising spin glass*, Phys.Rev. **B66**, 224419 (2002), [arXiv: cond-mat/0108307].
- [22] J.J. Moreno, H.G. Katzgraber, A.K. Hartmann, *Finding Low-Temperature States with Parallel Tempering, Simulated Annealing and Simple Monte Carlo*, Int.J.Mod.Phys. **14**, 285 (2003), [arXiv: cond-mat/0209248].
- [23] T.L. Veldhuizen, *Dynamic Multilevel Graph Visualization*, [arXiv:cs.GR/07121549].
- [24] <http://www.florianconrady.com/simulations.html>
- [25] L.V. Ahlfors, L. Sario, “Riemann Surfaces”, Princeton University Press, 1960.
- [26] W. Janke, D.A. Johnston, M. Weigel, *Two-dimensional quantum gravity — a laboratory for fluctuating graphs and quenched connectivity disorder*, Condens.Matter Phys. **9**, 263 (2006).
- [27] M. Reisenberger, C. Rovelli, *Spin foams as Feynman diagrams*, [arXiv:gr-qc/0002083].
- [28] M.P. Reisenberger and C. Rovelli, *Spacetime as a Feynman diagram: The connection formulation*, Class.Quant.Grav. **18** 121 (2001), [arXiv:gr-qc/0002095].
- [29] D. Oriti, *The group field theory approach to quantum gravity*, [arXiv:gr-qc/0607032].
- [30] C. Rovelli, F. Vidotto, *Single particle in quantum gravity and BGS entropy of a spin network*, Phys.Rev. **D81** 044038 (2010), [arXiv:0905.2983 [gr-qc]].